

# Implicit Regression in Subspace for High-Sensitivity CEST Imaging

## Appendix

### 1 Phantom Simulation

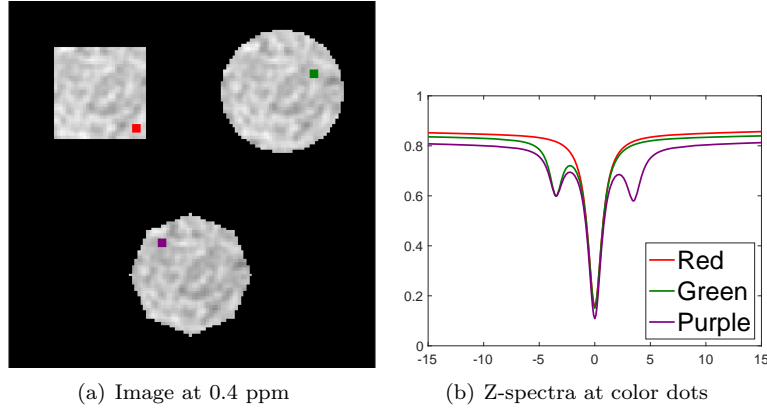


Figure 1: Synthetic phantom visualization.

We simulated three sets of z-spectra by varying the number of basis functions in the Lorentzian model [1, 2] as,

$$L(\Delta\omega) = c - l_{DS}(\Delta\omega) - l_{MT}(\Delta\omega) - l_{APT}(\Delta\omega) - l_{rNOE}(\Delta\omega), \quad (1)$$

where  $c$  is a constant,

$$l_{DS}(\Delta\omega) = \frac{A_{DS}}{1 + (\frac{\Delta\omega - \delta_{DS}}{\Gamma_{DS}/2})^2}, \quad (2)$$

$$l_m(\Delta\omega) = \frac{A_m}{1 + (\frac{\Delta\omega - \delta_{DS} - \delta_m}{\Gamma_m/2})^2}, m \in \{MT, APT, rNOE\}, \quad (3)$$

where  $\Delta\omega$  is chemical shift variable,  $c$  is a constant and  $\delta_{MT} = -2.5ppm$ ,  $\delta_{APT} = 3.5ppm$ ,  $\delta_{NOE} = -3.5ppm$ .

Parameter settings are shown in Table 1. The square phantom represented the direct water saturation with the MT effect, the circular phantom included

Table 1: Range of Randomized Parameters (MIN / MAX).

<b>Phantom</b>	Square	Circle	Octagon
$c$	0.8 / 1	0.8 / 1	0.8 / 1
$\delta_{DS}$	0	0	0
$A_{DS}$	0.6 / 0.8	0.6 / 0.8	0.6 / 0.8
$\Gamma_{DS}$	1 / 2	1 / 2	1 / 2
$A_{MT}$	0.01 / 0.1	0.01 / 0.1	0.01 / 0.1
$\Gamma_{MT}$	80 / 80	80 / 80	80 / 80
$A_{rNOE}$	0	0.1 / 0.3	0.1 / 0.3
$\Gamma_{rNOE}$	-	1 / 2	1 / 2
$A_{APT}$	0	0	0.1 / 0.3
$\Gamma_{APT}$	-	-	1 / 2

Table 2: Boundary and initial value settings for optimization in Eq. 4.

<b>Conditions</b>	Lower Bound	Upper Bound	Initial Value
$c$	0.9	1	1
$\delta_{DS}$	-0.2	0.2	0
$A_{DS}$	0.5	1	0.8
$\Gamma_{DS}$	1	10	6
$A_{MT}$	0.0025	0.2	0.1
$\Gamma_{MT}$	30	100	200
$A_{rNOE}$	0	0.3	0.1
$\Gamma_{rNOE}$	5	20	8
$A_{APT}$	0	0.4	0.3
$\Gamma_{APT}$	1	3	2

extra rNOE effect, and the octagonal phantom added the APT on top of the previous two effects. In addition, we applied Gaussian filtering to the randomly generated parameters in the Lorentzian model to mimic spatial variance and smoothness, where  $3 \times 3$  Gaussian kernel with  $\sigma = 1$  was used.

## 2 In-vivo 4-pool Lorentzian Fitting

CEST mapping was achieved by 4-pool Lorentzian fitting [2,3]. The same model in Eq. 1 was applied here for addressing the following non-linear least square problem,

$$\operatorname{argmin}_P \frac{1}{2} \|L_i(P; \Delta\omega) - Z_i(\Delta\omega)\|^2, i = 1, \dots, MN, \quad (4)$$

where  $M \times N$  is the spatial dimension of given data, and  $P$  is the group of parameters in the Lorentzian model being estimated. The optimization problem was solved by “levenberg-marquardt” method signal by signal, of which boundary condition and initial value settings are listed in Table. 2. The optimal  $A_{APT}$  and  $A_{rNOE}$  for each pixel are then formulated to  $APT$  (3.5ppm) and  $rNOE$  (-3.5ppm) maps respectively.

## References

- [1] Moritz Zaiss and Peter Bachert. Chemical exchange saturation transfer (cest) and mr z-spectroscopy in vivo: a review of theoretical approaches and methods. *Physics in Medicine & Biology*, 58(22):R221, 2013.
- [2] Steffen Goerke, Yannick Soehngen, Anagha Deshmane, Moritz Zaiss, Johannes Breitling, Philip S Boyd, Kai Herz, Ferdinand Zimmermann, Karel D Klika, Heinz-Peter Schlemmer, et al. Relaxation-compensated apt and rnoe cest-mri of human brain tumors at 3 t. *Magnetic resonance in medicine*, 82(2):622–632, 2019.
- [3] Felix Glang, Anagha Deshmane, Sergey Prokudin, Florian Martin, Kai Herz, Tobias Lindig, Benjamin Bender, Klaus Scheffler, and Moritz Zaiss. Deepcest 3t: Robust mri parameter determination and uncertainty quantification with neural networks—application to cest imaging of the human brain at 3t. *Magnetic Resonance in Medicine*, 84(1):450–466, 2020.